JOURNAL OF CHEMICAL INFORMATION AND MODELING

Letter

pubs.acs.org/jcim

From Determinants of RUNX1/ETO Tetramerization to Small-Molecule Protein−Protein Interaction Inhibitors Targeting Acute Myeloid Leukemia

Alexander Metz,[†,§] Julia Schanda,[‡,§] Manuel Grez,*[,‡,∥] Christian Wichmann,[‡,∥,#,*] and Holger Gohlke*[,†,∥]

[†]Institute for Pharmaceutical and Medicinal Chemistry, Department of Mathematics and Natural Sciences, Heinrich-Heine-University, Universitätsstr. 1, 40225 Düsseldorf, Germany

[‡]Institute for Biomedical Research, Georg-Speyer-Haus, Paul-Ehrlich-Str. 42-44, 60596 Frankfurt, Germany

Supporting Information

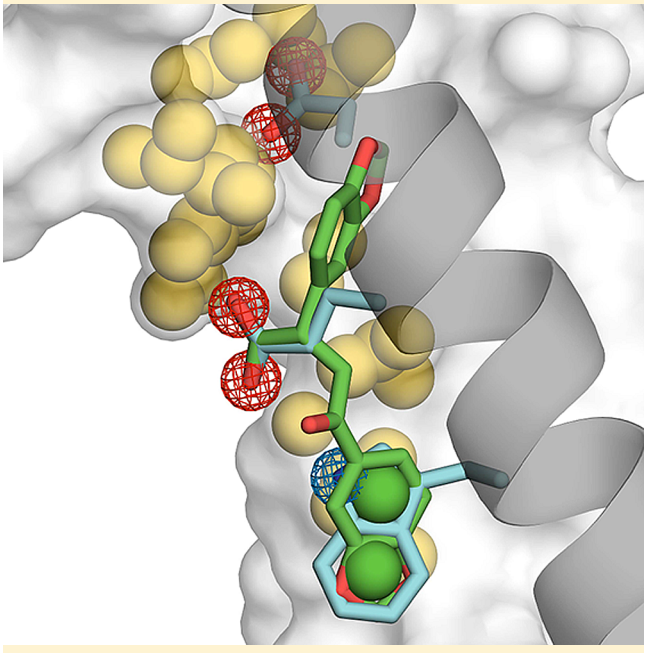

ABSTRACT: We identified the first small-molecule protein−protein interaction inhibitors of RUNX1/ETO tetramerization applying structure-based virtual screening guided by predicted hot spots and pockets in the interface. A 3D similarity screening revealed specific hot spot mimetics, one of which prevents the proliferation of RUNX1/ETO-dependent SKNO-1 cells at low micromolar concentration. Using solely a protein−protein complex structure to start with, this strategy can be the first step in any comparable structure-based endeavor to identify protein−protein interaction inhibitors.

The chromosomal translocation t(8;21) is frequently found in acute myeloid leukemia (AML).[2] This translocation involves the *RUNX1* gene, a key regulator of hematopoietic cell differentiation,[3] and the *ETO* gene, containing a nervy homology region 2 (NHR2) oligomerization domain.[4] Subsets of RUNX1/ETO-dependent AML are associated with unfavorable prognoses and high relapse rates after chemotherapy,[5] e.g., when coinciding with c-KIT mutations.[2] We and others demonstrated that homotetramerization of the α-helical NHR2 domain of the RUNX1/ETO fusion protein (also AML1/ETO) is an essential prerequisite for the onset and maintenance of AML.[1,4,6−8] Recently, the NHR2 containing CBFA2T3/GLIS2 fusion protein has been linked to an aggressive subtype of pediatric acute megakaryoblastic leukemia.[9,10] Thus, interfering with NHR2-mediated tetramerization in oncoproteins is an attractive strategy for molecular intervention and personalized therapy.[11,12]

We reported a 128mer fusion protein containing the complete NHR2 domain (NC128) that disrupts RUNX1/ETO tetramerization and counteracts leukemic cell characteristics.[11] Likewise, a cell-penetrating TAT-NHR2 fusion protein interferes with the leukemogenic function of RUNX1/ETO.[13] While providing a proof-of-principle for the molecular disruption of RUNX1/ETO tetramerization, these fusion proteins lack favorable ADME properties. Thus, we set out to identify small-molecule protein−protein interaction inhibitors (PPII) with the same mode of action but better pharmacokinetic properties.

The NHR2 tetramer is a symmetric dimer of dimers, each of which contains two extended α-helical monomers that associate in a head-to-tail orientation to form a four-helix bundle (Figure 1a).[4] Targeting such protein−protein interactions (PPI) is considered difficult because of the size, lack of deep binding pockets, and stability of PPI.[14] However, the widespread identification of (drug-like) PPII demonstrates that this challenge can be overcome.[15,16] Often PPII act by targeting a subregion of the interface that contains hot spots and pockets.[16,17]

Here, we report the first PPII of RUNX1/ETO tetramerization that prevent the proliferation of RUNX1/ETO-dependent cells and were identified by a combination of computational and experimental methods. Key to this success was a computational strategy we introduced recently (Figure 1).[18] This strategy starts from the structure of a protein−protein complex and simultaneously considers aspects of energetics and plasticity relevant for PPII binding to an interface. Hence, we analyzed the energetic contribution of individual amino acids to the NHR2 dimer−tetramer transition (tetramerization) by a structural decomposition of a computed binding free energy[19] and predicted a cluster of five amino acids (W498, W502,

Published: August 19, 2013

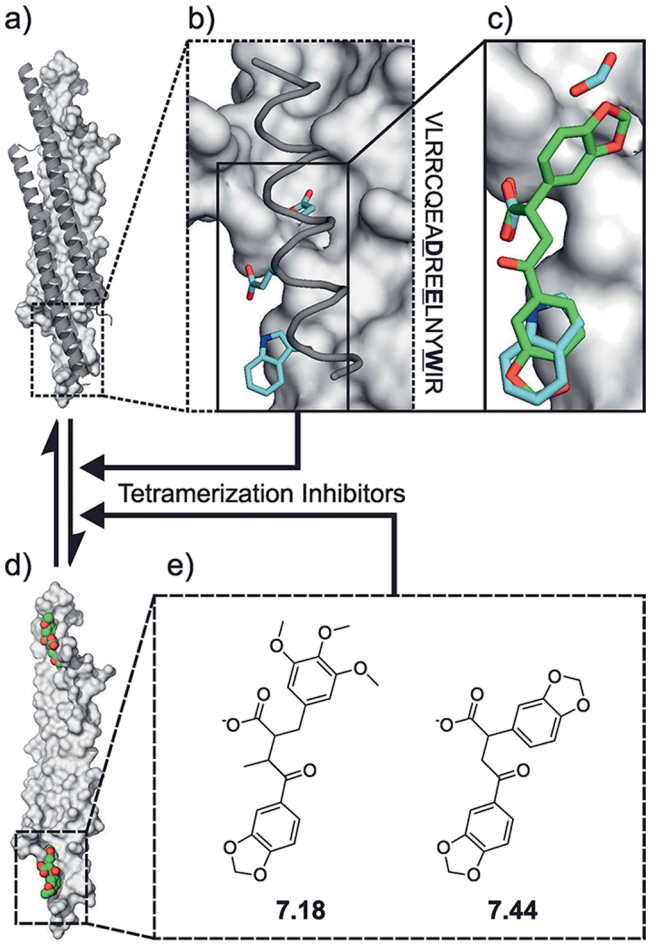

Figure 1. Identification of inhibitors of NHR2 tetramerization. (a) Starting from the NHR2 tetramer (PDB: 1wq6[4]) we derived an (b) inhibitory peptide (**P1**, ribbon) carrying three previously identified hot spots of NHR2 tetramerization (cyan; highlighted in the sequence).[1] (c) Small molecules were screened by ROCS for their ability to mimic the hot spot pattern (**7.44** superimposed with query (III)). (d) This led to the identification of inhibitors of NHR2 tetramerization that are proposed to bind to either one of the two equivalent binding regions in the interface of the NHR2 dimer. (e) The most potent inhibitors of NHR2 tetramerization **7.18** and **7.44**.

D533, E536, W540; RUNX1/ETO sequence numbering; Figure S1, Supporting Information) with strong contributions to the stability of the tetramer ("hot spots").[1]

Mutating the hot spots to alanine abolishes tetramer formation without affecting the dimer formation or helicity of NHR2.[1] Moreover, RUNX1/ETO dimers do not block myeloid differentiation, are unable to enhance the self-renewal capacity of hematopoietic progenitors, and fail to induce leukemia in a murine transplantation model.[1] Scanning the NHR2 dimer–dimer interface[20] revealed the deepest and largest pocket (269 Å^3; Figure S1a, Supporting Information), which is still rather shallow compared to binding sites in conventional[21,22] and other protein–protein[23] targets. Yet, pockets are considered important for the high-affinity binding of PPII.[16,24] Considering that this pocket is close to the cluster of identified hot spots and even binds the most important hot spot D533,[1] our analyses revealed an essential structural motif in the NHR2 interface that is suitable for intervention in t(8;21) leukemia.[1]

While structure-based drug design approaches previously helped identifying PPII,[25,26] mostly starting from peptide or ligand-bound structures, we decided to proceed with the structure-based identification of inhibitors of the NHR2 tetramerization based on the essential structural motif. Further analyses of the five hot spots suggested D533, E536, and W540 as the most suitable template motif (Figure 1b) for the following reasons: these hot spots decorate one face of each α-helix of an NHR2 dimer, project side chains from sequence positions i, i+3, and i+7 similar to known helix mimetics,[27−29] cluster sufficiently close together to be replaced by a drug-like molecule,[16] and extend into the deepest pocket of the NHR2 interface. In addition, they contact the NHR2 interface by a balanced mix of charged/acceptor (D533, E536) and aromatic/donor (W540) interactions. This would allow mimetics of the hot spots to be less hydrophobic than the common helix mimetic scaffolds[27,28,30] and offer more specificity for binding than purely hydrophobic interactions.

On the basis of this template motif, we suggested the 18mer peptide **P1** as an inhibitor of NHR2 tetramerization. **P1** was derived from the NHR2 domain (Figure 1b; Figure S2a, Supporting Information) and encloses the template motif. The N-terminal 12mer peptide (Ac-EA**D**RE**E**LNY**W**IR-NH$_2$) has an α-helical content of ∼35% as determined by circular dichroism spectroscopy (Figure S3, Supporting Information). Convincingly, BS^3 cross-linking experiments revealed that **P1** inhibits the NHR2 tetramerization with IC$_{50}$ ≈ 250 μM (Figure 2a–c). The moderate IC$_{50}$ reflects the competition of **P1** against the strong tendency of NHR2 dimers to self-associate. The NHR2 tetramer has a melting point of 85 °C,[1] and we could not detect unbound dimers for any construct containing the wild type NHR2 domain by either size-exclusion chromatography or analytical ultracentrifugation.[1] Still, this data provides the first proof-of-principle that the NHR2 tetramerization can be inhibited by a molecule significantly smaller than the NHR2 domain itself.

Further BS^3 cross-linking experiments revealed that alanine mutations of the three hot spot residues in **P1** (resulting in peptide **P2**) or another two interface residues projecting toward the interface (peptide **P3**) abolish the inhibitory effect (Figure 2a). As these results reconfirmed the importance of the hot spot residues, we used this information together with the structural knowledge of the location and orientation of these residues' side chains in the crystal structure in a virtual screening (VS) for PPII mimicking the hot spot interactions.

To this end, we built three queries (Figure S4, Supporting Information) containing (I) only the carboxylic and indole functional groups of D533, E536, and W540, (II) a terpyridine helix mimetic[29] decorated with the functional groups from (I) and with the terpyridine modeled in the position of the helix that should be replaced, or (III) the functional groups from (I) plus repulsive Gaussian potentials centered on all adjacent protein interface atoms (≤ 4 Å distance) to penalize molecules clashing with the interface. With these queries, we searched the refined (Supporting Information) purchasable subset of the ZINC 11 database.[31] We screened ∼6 × 10^6 molecules with ROCS (Rapid Overlay of Chemical Structures)[32] that superimposes molecules based on a 3D overlap of molecular shape and donor, acceptor, anionic, cationic, hydrophobic, and aromatic (ring) properties, referred to as colors.

We performed three ROCS searches on the conformers, one for each query. Also, to account for the conformational variability of the target and the template motif, each search was

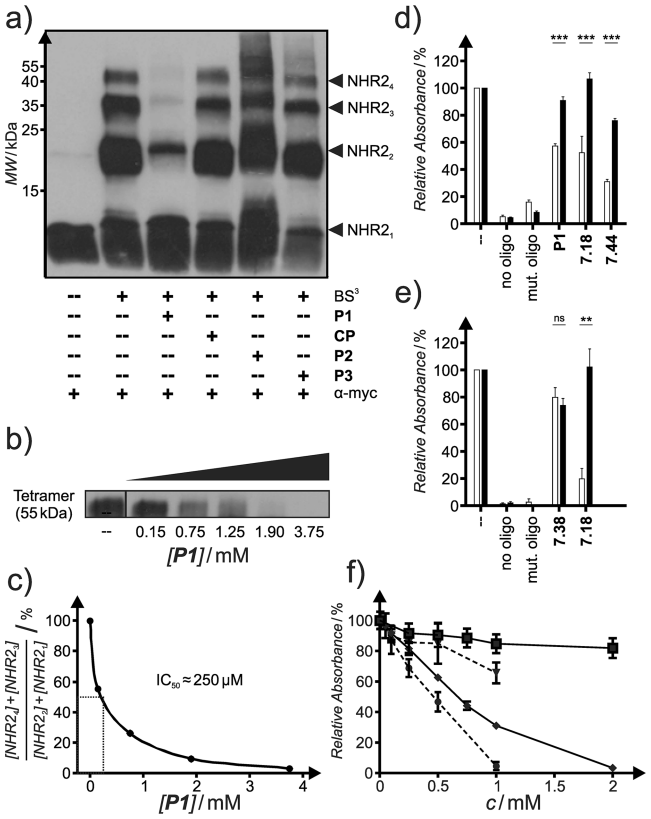

Figure 2. Inhibition of NHR2 tetramerization. (a) Peptide **P1**, but neither **P2**, **P3**, nor the unrelated peptide **CP** inhibit NHR2 tetramerization as shown by the reduction of BS^3 cross-linked NHR2 oligomers (c = 1100 μM). (b) The inhibition by **P1** is dose-dependent (c) with $IC_{50} \approx 250$ μM. (d) ELISA and (e) ABCD experiments show that **P1**, **7.18**, and **7.44**, but not **7.38**, selectively inhibit tetramer-dependent binding of the RUNX1-NHR2 protein (white bars) to an immobilized RUNX3 oligonucleotide while binding of the RUNX1-BCR protein (black bars) is not inhibited ([P1] = 500 μM and [PPII] = 2000 μM in ELISA; [PPII] = 1000 μM in ABCD assay). (f) Dose-dependent inhibition of RUNX1-NHR2 tetramerization in the ELISA by **P1** (●; IC_{50} = 390 ± 30 μM) and **7.44** (◆ ; IC_{50} = 630 ± 24 μM) but neither by **P3** (▼) nor by **7.38** (■). Standard deviations for $n \geq 2$. ns: not significant. **: $0.01 > p \geq 0.001$. ***: $p < 0.0001$ (unpaired t-test).

performed independently using side chain conformations of the hot spots from either end of the NHR2 interface. These interface conformations differ by a root-mean-square deviation (RMSD) of 0.3 Å (Figure S1b,c, Supporting Information). All ROCS results were reranked exclusively by color overlap to favor compounds that optimally mimic the hot spot functional groups. For each search, the top scoring ZINC entries of either set of side chain conformations were combined; duplicates were removed.

The resulting poses vividly illustrate to what extent substructures of compounds overlap with the functional groups of the hot spots (Figure 1c; Figure S4d–f, Supporting Information). We assessed the 1000 top scoring compound poses for each query visually based on interaction complementarity, steric overlap with the targeted interface and the helix to be replaced, conformational strain, and structural diversity. Finally, we selected 80 compounds (Table S1, Supporting Information) for experimental testing.

We measured the inhibition of NHR2 tetramerization in vitro by tetramer-dependent binding of a RUNX1-NHR2 protein construct (Figure 2; Figure S2b, Supporting Information) to an immobilized oligonucleotide, which was derived from the RUNX3 promoter sequence, in ELISA and ABCD assays[33] (Figure 2d–f; Figures S5 and S6 and Table S2, Supporting Information). Seven compounds showed consistent and selective inhibition in both assays (Table S2, Supporting Information) with activities comparable to **P1** (42.8% inhibition at c = 500 μM and IC_{50} = 390 ± 30 μM by ELISA; Figure 2f; Figure S7, Supporting Information). The most promising compound **7.18** (Figure 1e) showed an NHR2 inhibition of 80.3% (c = 1 mM) in the ABCD and 47.7% (c = 2 mM) in the ELISA assay (Table S2, Supporting Information) but was inactive in cells. Selectivity for NHR2 was demonstrated by the reduced inhibition when replacing the NHR2 domain of the construct with the homologous BCR tetramerization domain (RUNX1-BCR protein; Figure 2; Figure S2b, Supporting Information); this finding also suggests that the observed inhibition of NHR2 tetramerization in RUNX1-NHR2 does not occur due to nonspecific protein binding.

Structurally, **7.18** contains a central 4-oxobutanoic acid scaffold substituted by a 4-(1,3-benzodioxolyl) and a 2-(3,4,5-trimethoxy-benzyl) moiety (Figure 1e). The ROCS pose shows how **7.18** mimics the template motif. The PPII's carboxylate group mimics that of E536, while the benzodioxolyl and trimethoxybenzyl moieties mimic the indole of W540 and the carboxylate of D533, respectively (Figure S4d, Supporting Information).

Next, a fingerprint similarity search[34] for structural analogs of **7.18** in the refined database[31] revealed **7.44** with improved in vitro activity (IC_{50} = 630 ± 24 μM by ELISA; Figure 2; Figure S7, Supporting Information). This activity is only 1.6-fold lower than that of **P1**. The related Hill coefficient for **7.44** is 1.8, which does not contradict the assumed inhibitory mechanism: Once a first PPII interferes with NHR2 tetramer formation, the second symmetry-related binding site on the NHR2 dimer becomes more easily accessible such that the affinity for the second PPII increases. Notably, for **P1** a similar Hill coefficient of 1.9 is found (Figure S7, Supporting Information), suggesting a common mechanism for both inhibitors as expected. Furthermore, **7.44** selectively reduced the viability of RUNX1/ETO-dependent human leukemic SKNO-1 cells (EC_{50} < 10 μM) in accord with the effect of NC128,[11] whereas treatment of these cells with inactive **7.38** or of RUNX1/ETO-independent U937 cells with **7.44** had no effect (Figure 3).

The improved activity can be explained by comparing the ROCS poses of **7.18** and **7.44** (Figure S4d–f, Supporting Information). **7.44** overlaps less with the protein by replacing the trimethoxybenzyl of **7.18** by a shorter, more compact, less flexible, and hence also entropically more favorable second benzodioxolyl moiety that mimics the carboxylate of D533 (Figure 1c). The ROCS ranks suggest a preferred binding of the 2*S* stereoisomers of **7.18** and **7.44**. In addition, a reversed binding mode is found for **7.44** by ROCS (Figure S4f, Supporting Information). Crystal structure analyses[35,36] and a search in the SwissBioisostere database[37] support this mimicry of both carboxylate and indole groups by 1,3-benzodioxoles. The proposed binding modes will help suggesting further modifications of these lead compounds. In that respect, both PPII are good starting points for optimization due to their low molecular weight (**7.18**: 415 Da; **7.44**: 341 Da), simple chemical structure, and ligand efficiency ($LE_{7.44}$ = −0.18

dx.doi.org/10.1021/ci400332e | J. Chem. Inf. Model. 2013, 53, 2197−2202

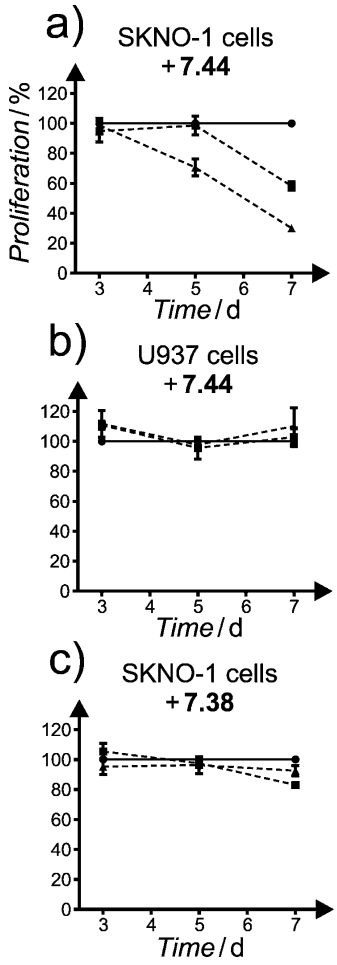

Figure 3. NHR2 inhibitor **7.44** specifically reduces proliferation of RUNX1/ETO-dependent cells. SKNO-1 cell or U937 cells were treated with 1 μM (■) or 10 μM (▲) of **7.44** or **7.38** or no PPII (●). (a) RUNX1/ETO-dependent SKNO-1 cells were severely affected by **7.44** (b) while RUNX1/ETO-independent U937 cells were unaffected. **7.38**, inactive in vitro, did not affect SKNO-1 cells. Proliferation measured by XTT assay. Standard deviations for $n \geq 3$.

kcal mol^{-1} related to the IC_{50}) that is already similar to PPII employed in the clinics.[16,38]

7.44 was recently shown to inhibit c-Jun N-terminal kinase (JNK) and affect the JNK-pathway in cells.[39] This may provide an explanation as to why **7.44** reduces the viability of RUNX1/ETO-dependent SKNO-1 cells at an EC_{50} value much lower than the IC_{50} value found in in vitro experiments on the inhibition of NHR2 tetramerization (see above). In turn, our results indicate that **7.44** could exert an additional effect on the JNK-pathway in that RUNX1/ETO-mediated activation of the JNK-pathway[40,41] can also be inhibited by inhibition of NHR2 tetramerization, as demonstrated by the absence of c-Jun upregulation in the case of RUNX1/ETO with hot spot residues mutated to alanine.[1] Finally, the study excluded the possibility of unspecific protein binding of **7.44** in terms of aggregates as did it exclude an unspecific action of **7.44** as a redox cycling compound.[39] **7.44** is structurally similar to (epi)podophyllotoxins; the latter are non-intercalating inhibitors of topoisomerase II[36] and microtubule formation.[42] We can exclude that **7.44** acts that way because of the absence of the respective targets in our ELISA and ABCD assays.

In summary, from the determinants of NHR2 tetramerization[1] previously revealed by computational hot spot[18] and pocket prediction,[20] a molecular recognition pattern at the NHR2 dimer interface was defined. This pattern successfully guided VS resulting in the first small-molecule inhibitors of NHR2 tetramerization, one of which prevents the proliferation of RUNX1/ETO-dependent SKNO-1 cells at a low micromolar concentration. These results could guide further efforts to intervene with RUNX1/ETO-positive AML and other NHR2 tetramerization-dependent mechanisms. Our results furthermore demonstrate that by this computational strategy small-molecule PPII can be identified even in cases where nothing else than a protein−protein complex structure is known. Hence, this strategy can be the first step in any comparable structure-based endeavor to identify PPII.

■ ASSOCIATED CONTENT

Supporting Information

Tables with the tested substances (Table S1) and the in vitro inhibition of NHR2 tetramerization (Table S2) as well as graphical representations of the hot spot containing region of the NHR2 interface (Figure S1), experimentally tested peptides and proteins (Figure S2), helical content of the inhibitory 12mer peptide (Figure S3), ROCS queries used for VS and exemplary ROCS poses of the most active inhibitors (Figure S4), biochemical assays for measuring inhibition of NHR2 tetramerization (Figure S5), ELISA screening results for inhibitors of RUNX1/ETO tetramerization (Figure S6), and the dose-dependent inhibition of RUNX1-NHR2 tetramerization in the ELISA (Figure S7). This material is available free of charge via the Internet at http://pubs.acs.org.

■ AUTHOR INFORMATION

Corresponding Authors

*E-mail: grez@gsh.uni-frankfurt.de (M.G.).
*E-mail: christian.wichmann@med.uni-muenchen.de (C.W.).
*E-mail: gohlke@uni-duesseldorf.de (H.G.). Fax: (+49) 211-8113847 (H.G.).

Present Address

[#](C.W.) Department of Transfusion Medicine, Cell Therapeutics and Hemostasis, Ludwig-Maximilian University Hospital, Munich, Germany.

Author Contributions

[§]These authors contributed equally to this work.

Notes

The authors declare no competing financial interest.
[∥]These authors share senior authorship.

■ ACKNOWLEDGMENTS

We are grateful for financial support from the NGFNplus Cancer Network (Grant 01GS0879), Deutsche Krebshilfe (Grant 102362, TP7), LOEWE Center for Cell and Gene Therapy Frankfurt (HMWK III L 4-518/17.004 [2010]), "Strategischer Forschungsfonds" at Heinrich-Heine-University, and "Kind-Philipp-Stiftung"; for computational support by the "Zentrum für Informations und Medientechnologie" at the Heinrich-Heine-University; to the NCI/DTP Open Chemical Repository (http://dtp.cancer.gov/) for compound samples; and to OpenEye for an academic license.

■ ABBREVIATIONS

ABCD assay, avidin−biotin complex DNA assay; AML, acute myeloid leukemia; ELISA, enzyme-linked immunosorbent assay; JNK, c-Jun N-terminal kinase; NHR2, nervy homology region 2; PPI, protein−protein interaction; PPII, protein−protein interaction inhibitor; RMSD, root-mean-square deviation; ROCS, rapid overlay of chemical structures; VS, virtual screening

■ REFERENCES

(1) Wichmann, C.; Becker, Y.; Chen-Wichmann, L.; Vogel, V.; Vojtkova, A.; Herglotz, J.; Moore, S.; Koch, J.; Lausen, J.; Mantele, W.; Gohlke, H.; Grez, M. Dimer-tetramer transition controls RUNX1/ETO leukemogenic activity. *Blood* **2010**, *116* (4), 603−613.

(2) Reikvam, H.; Hatfield, K. J.; Kittang, A. O.; Hovland, R.; Bruserud, O. Acute myeloid leukemia with the t(8;21) Translocation: Clinical consequences and biological implications. *J. Biomed. Biotechnol.* **2011**, *104631*, 1−23.

(3) Tenen, D. G. Disruption of differentiation in human cancer: AML shows the way. *Nat. Rev. Cancer* **2003**, *3* (2), 89−101.

(4) Liu, Y.; Cheney, M. D.; Gaudet, J. J.; Chruszcz, M.; Lukasik, S. M.; Sugiyama, D.; Lary, J.; Cole, J.; Dauter, Z.; Minor, W.; Speck, N. A.; Bushweller, J. H. The tetramer structure of the nervy homology two domain, NHR2, is critical for AML1/ETO's activity. *Cancer Cell* **2006**, *9* (4), 249−260.

(5) Shimada, A.; Taki, T.; Tabuchi, K.; Tawa, A.; Horibe, K.; Tsuchida, M.; Hanada, R.; Tsukimoto, I.; Hayashi, Y. KIT mutations, and not FLT3 internal tandem duplication, are strongly associated with a poor prognosis in pediatric acute myeloid leukemia with t(8;21): A study of the Japanese Childhood AML Cooperative Study Group. *Blood* **2006**, *107* (5), 1806−1809.

(6) Ptasinska, A.; Assi, S. A.; Mannari, D.; James, S. R.; Williamson, D.; Dunne, J.; Hoogenkamp, M.; Wu, M.; Care, M.; McNeill, H.; Cauchy, P.; Cullen, M.; Tooze, R. M.; Tenen, D. G.; Young, B. D.; Cockerill, P. N.; Westhead, D. R.; Heidenreich, O.; Bonifer, C. Depletion of RUNX1/ETO in t(8;21) AML cells leads to genome-wide changes in chromatin structure and transcription factor binding. *Leukemia* **2012**, *26* (1), 1829−1841.

(7) Rhoades, K. L.; Hetherington, C. J.; Harakawa, N.; Yergeau, D. A.; Zhou, L. M.; Liu, L. Q.; Little, M. T.; Tenen, D. G.; Zhang, D. E. Analysis of the role of AML1-ETO in leukemogenesis, using an Inducible transgenic mouse model. *Blood* **2000**, *96* (6), 2108−2115.

(8) Heidenreich, O.; Krauter, J.; Riehle, H.; Hadwiger, P.; John, M.; Heil, G.; Vornlocher, H. P.; Nordheim, A. AML1/MTG8 oncogene suppression by small interfering RNAs supports myeloid differentiation of t(8;21)-positive leukemic cells. *Blood* **2003**, *101* (8), 3157−3163.

(9) Gruber, T. A.; Larson Gedman, A.; Zhang, J.; Koss, C. S.; Marada, S.; Ta, H. Q.; Chen, S. C.; Su, X.; Ogden, S. K.; Dang, J.; Wu, G.; Gupta, V.; Andersson, A. K.; Pounds, S.; Shi, L.; Easton, J.; Barbato, M. I.; Mulder, H. L.; Manne, J.; Wang, J.; Rusch, M.; Ranade, S.; Ganti, R.; Parker, M.; Ma, J.; Radtke, I.; Ding, L.; Cazzaniga, G.; Biondi, A.; Kornblau, S. M.; Ravandi, F.; Kantarjian, H.; Nimer, S. D.; Dohner, K.; Dohner, H.; Ley, T. J.; Ballerini, P.; Shurtleff, S.; Tomizawa, D.; Adachi, S.; Hayashi, Y.; Tawa, A.; Shih, L. Y.; Liang, D. C.; Rubnitz, J. E.; Pui, C. H.; Mardis, E. R.; Wilson, R. K.; Downing, J. R. An Inv(16)(p13.3q24.3)-encoded CBFA2T3-GLIS2 fusion protein defines an aggressive subtype of pediatric acute megakaryoblastic leukemia. *Cancer Cell* **2012**, *22* (5), 683−697.

(10) Thiollier, C.; Lopez, C. K.; Gerby, B.; Ignacimouttou, C.; Poglio, S.; Duffourd, Y.; Guegan, J.; Rivera-Munoz, P.; Bluteau, O.; Mabialah, V.; Diop, M.; Wen, Q.; Petit, A.; Bauchet, A. L.; Reinhardt, D.; Bornhauser, B.; Gautheret, D.; Lecluse, Y.; Landman-Parker, J.; Radford, I.; Vainchenker, W.; Dastugue, N.; de Botton, S.; Dessen, P.; Bourquin, J. P.; Crispino, J. D.; Ballerini, P.; Bernard, O. A.; Pflumio, F.; Mercher, T. Characterization of novel genomic alterations and therapeutic approaches using acute megakaryoblastic leukemia xenograft models. *J. Exp. Med.* **2012**, *209* (11), 2017−2031.

(11) Wichmann, C.; Chen, L. P.; Heinrich, M.; Baus, D.; Pfitzner, E.; Zornig, M.; Ottmann, O. G.; Grez, M. Targeting the oligomerization domain of ETO interferes with RUNX1/ETO oncogenic activity in t(8;21)-positive leukemic cells. *Cancer Res.* **2007**, *67* (5), 2280−2289.

(12) Sun, X. J.; Wang, Z.; Wang, L.; Jiang, Y.; Kost, N.; Soong, T. D.; Chen, W. Y.; Tang, Z.; Nakadai, T.; Elemento, O.; Fischle, W.; Melnick, A.; Patel, D. J.; Nimer, S. D.; Roeder, R. G. A stable transcription factor complex nucleated by oligomeric AML1-ETO controls leukaemogenesis. *Nature* **2013**, *500* (7460), 93−97.

(13) Bartel, Y.; Grez, M.; Wichmann, C. Interference with RUNX1/ETO leukemogenic function by cell-penetrating peptides targeting the NHR2 oligomerization domain. *Biomed. Res. Int.* **2013**, *2013*, 297692.

(14) Surade, S.; Blundell, T. L. Structural biology and drug discovery of difficult targets: The limits of ligandability. *Chem. Biol.* **2012**, *19* (1), 42−50.

(15) Zinzalla, G.; Thurston, D. E. Targeting protein−protein interactions for therapeutic intervention: A challenge for the future. *Future Med. Chem.* **2009**, *1* (1), 65−93.

(16) Metz, A.; Ciglia, E.; Gohlke, H. Modulating protein−protein interactions: From structural determinants of binding to druggability prediction to application. *Curr. Pharm. Des.* **2012**, *18*, 4630−4647.

(17) Moreira, I. S.; Fernandes, P. A.; Ramos, M. J. Hot spots: A review of the protein−protein interface determinant amino-acid residues. *Proteins: Struct., Funct., Bioinf.* **2007**, *68* (4), 803−812.

(18) Metz, A.; Pfleger, C.; Kopitz, H.; Pfeiffer-Marek, S.; Baringhaus, K. H.; Gohlke, H. Hot spots and transient pockets: Predicting the determinants of small-molecule binding to a protein−protein interface. *J. Chem. Inf. Model.* **2012**, *52* (1), 120−133.

(19) Gohlke, H.; Kiel, C.; Case, D. A. Insights into protein−protein binding by binding free energy calculation and free energy decomposition for the Ras-Raf and Ras-RaIGDS complexes. *J. Mol. Biol.* **2003**, *330* (4), 891−913.

(20) Craig, I. R.; Pfleger, C.; Gohlke, H.; Essex, J. W.; Spiegel, K. Pocket-space maps to identify novel binding-site conformations in proteins. *J. Chem. Inf. Model.* **2011**, *51* (10), 2666−2679.

(21) Kahraman, A.; Morris, R. J.; Laskowski, R. A.; Thornton, J. M. Shape variation in protein binding pockets and their ligands. *J. Mol. Biol.* **2007**, *368* (1), 283−301.

(22) Perot, S.; Sperandio, O.; Miteva, M. A.; Camproux, A. C.; Villoutreix, B. O. Druggable pockets and binding site centric chemical space: a paradigm shift in drug discovery. *Drug Discovery Today* **2010**, *15* (15−16), 656−667.

(23) Eyrisch, S.; Helms, V. Transient pockets on protein surfaces involved in protein−protein interaction. *J. Med. Chem.* **2007**, *50* (15), 3457−3464.

(24) Higueruelo, A. P.; Schreyer, A.; Bickerton, G. R. J.; Pitt, W. R.; Groom, C. R.; Blundell, T. L. Atomic interactions and profile of small molecules disrupting protein−protein interfaces: The TIMBAL Database. *Chem Biol Drug Des* **2009**, *74* (5), 457−467.

(25) Geppert, T.; Bauer, S.; Hiss, J. A.; Conrad, E.; Reutlinger, M.; Schneider, P.; Weisel, M.; Pfeiffer, B.; Altmann, K. H.; Waibler, Z.; Schneider, G. Immunosuppressive small molecule discovered by structure-based virtual screening for inhibitors of protein−protein interactions. *Angew Chem, Int Ed* **2012**, *51* (1), 258−261.

(26) Mukherjee, P.; Desai, P.; Zhou, Y. D.; Avery, M. Targeting the BH3 domain mediated protein−protein interaction of Bcl-xL through virtual screening. *J Chem Inf Model* **2010**, *50* (5), 906−923.

(27) Kim, I. C.; Hamilton, A. D. Diphenylindane-based proteomimetics reproduce the projection of the i, i+3, i+4, and i+7 residues on an alpha-helix. *Org. Lett.* **2006**, *8* (9), 1751−1754.

(28) Yin, H.; Hamilton, A. D. Strategies for targeting protein−protein interactions with synthetic agents. *Angew. Chem., Int. Ed.* **2005**, *44* (27), 4130−4163.

(29) Davis, J. M.; Truong, A.; Hamilton, A. D. Synthesis of a 2,3′;6′,3″-terpyridine scaffold as an alpha-helix mimetic. *Org. Lett.* **2005**, *7* (24), 5405−5408.

(30) Cummings, C. G.; Hamilton, A. D. Disrupting protein-protein interactions with non-peptidic, small molecule alpha-helix mimetics. *Curr. Opin. Chem. Biol.* **2010**, *14* (3), 341−346.

(31) Irwin, J. J.; Shoichet, B. K. ZINC–A free database of commercially available compounds for virtual screening. *J. Chem. Inf. Model.* **2005**, *45* (1), 177−182.
(32) *OEChem*, version 1.7.2; OpenEye Scientific Software, Inc.: Santa Fe, NM, 2009.
(33) McKay, I. A.; Kirby, L.; Volyanik, E. V.; Kumar, V.; Wong, P. W. Y.; Bustin, S. A. An enzyme-linked immunosorbent assay for the detection of agents which interfere with the DNA binding activities of transcription factors - Exemplified by NF-IL6. *Anal. Biochem.* **1998**, *265* (1), 28−34.
(34) Bender, A.; Mussa, H. Y.; Glen, R. C.; Reiling, S. Similarity searching of chemical databases using atom environment descriptors (MOLPRINT 2D): Evaluation of performance. *J. Chem. Inf. Comput. Sci.* **2004**, *44* (5), 1708−1718.
(35) Davey, D. D.; Adler, M.; Arnaiz, D.; Eagen, K.; Erickson, S.; Guilford, W.; Kenrick, M.; Morrissey, M. M.; Ohlmeyer, M.; Pan, G.; Paradkar, V. M.; Parkinson, J.; Polokoff, M.; Saionz, K.; Santos, C.; Subramanyam, B.; Vergona, R.; Wei, R. G.; Whitlow, M.; Ye, B.; Zhao, Z. S.; Devlin, J. J.; Phillips, G. Design, synthesis, and activity of 2-imidazol-1-ylpyrimidine derived inducible nitric oxide synthase dimerization inhibitors. *J. Med. Chem.* **2007**, *50* (6), 1146−1157.
(36) Wu, C. C.; Li, T. K.; Farh, L.; Lin, L. Y.; Lin, T. S.; Yu, Y. J.; Yen, T. J.; Chiang, C. W.; Chan, N. L. Structural basis of type II topoisomerase inhibition by the anticancer drug etoposide. *Science* **2011**, *333* (6041), 459−462.
(37) Wirth, M.; Zoete, V.; Michielin, O.; Sauer, W. H. B. SwissBioisostere: A database of molecular replacements for ligand design. *Nucleic Acids Res.* **2013**, *41* (D1), D1137−D1143.
(38) Wells, J. A.; McClendon, C. L. Reaching for high-hanging fruit in drug discovery at protein−protein interfaces. *Nature* **2007**, *450* (7172), 1001−1009.
(39) Kaoud, T. S.; Yan, C.; Mitra, S.; Tseng, C. C.; Jose, J.; Taliaferro, J. M.; Tuohetahuntila, M.; Devkota, A.; Sammons, R.; Park, J.; Park, H.; Shi, Y.; Hong, J.; Ren, P.; Dalby, K. N. From in silico discovery to intra-cellular activity: Targeting JNK-protein interactions with small molecules. *ACS Med. Chem. Lett.* **2012**, *3* (9), 721−725.
(40) Elsasser, A.; Franzen, M.; Kohlmann, A.; Weisser, M.; Schnittger, S.; Schoch, C.; Reddy, V. A.; Burel, S.; Zhang, D. E.; Ueffing, M.; Tenen, D. G.; Hiddemann, W.; Behre, G. The fusion protein AML1-ETO in acute myeloid leukemia with translocation t(8;21) induces c-jun protein expression via the proximal AP-1 site of the c-jun promoter in an indirect, JNK-dependent manner. *Oncogene* **2003**, *22* (36), 5646−5657.
(41) Gao, F. H.; Wang, Q.; Wu, Y. L.; Li, X.; Zhao, K. W.; Chen, G. Q. c-Jun N-terminal kinase mediates AML1-ETO protein-induced connexin-43 expression. *Biochem. Biophys. Res. Commun.* **2007**, *356* (2), 505−511.
(42) Srivastava, V.; Negi, A. S.; Kumar, J. K.; Gupta, M. M.; Khanuja, S. P. S. Plant-based anticancer molecules: A chemical and biological profile of some important leads. *Bioorg. Med. Chem.* **2005**, *13* (21), 5892−5908.